Rare-Earth Ions in the Alkali Halides. I. Emission Spectra of Sm^{2+}-Vacancy Complex

W. E. Bron and W. R. Heller*
IBM Watson Research Center, Yorktown Heights, New York
(Received 13 July 1964)

Measurements have been made of the crystal-field splitting of the ^7F_J energy levels of the $4f^6$ configuration of the Sm^{2+} ion which is dissolved in a number of alkali-halide lattices. Crystal-field term assignments were made from the results of polarized-emission measurements. Observed crystal-field splittings are compared to those predicted from point-charge models. Contributions to the total crystal field are considered to include that due to the presence of a nearest-neighbor cation vacancy as well as that due to displacements, from normal lattice positions, of the nearest-neighbor halide ions and the Sm^{2+} ion. The splitting is shown to arise in part from a displacement of the Sm^{2+} and the cation vacancy toward each other. The extent of the validity of the use of a point-charge model for this case is discussed.

INTRODUCTION

INTRODUCTION of a divalent cation into an alkali-halide lattice results in the formation of complexes of the divalent cation and a cation vacancy. The positive-ion lattice vacancy is present for charge compensation. Because of a distribution in the binding energy between the divalent impurity and the vacancy, the vacancies are expected to be distributed as nearest neighbors (n.n.), next-nearest neighbors (n.n.n.), and so on, about the impurity. These complexes have received considerable attention both theoretically[1] and through experiments on electron spin resonance,[2] dielectric loss,[3,4] ionic conductivity,[5] and mechanical relaxation.[6] The present work uses the crystal-field splitting of optically determined energy levels of the divalent samarium ion to study particularly the symmetry and magnitude of the crystal field about the Sm^{2+} ion and its associated vacancy. The choice of Sm^{2+} was dictated by the requirement of a divalent ion which can be dissolved in an alakali-halide lattice and which has optical spectral lines of the order of 1 Å in width so that small crystal-field splittings can be easily detected.

Figure 1 illustrates the n.n. complex. As can be seen from the figure, the impurity-vacancy axis is a twofold rotational axis which lies along the ⟨110⟩ direction of the alkali-halide lattice. The full symmetry is C_{2v}, since the defect lacks a center of inversion. A number of ionic displacements from normal lattice positions should occur in the vicinity of the defect owing to charge and size differences between the defect and the normal lattice ion.

Bassani and Fumi[1] have calculated the displacements of the halide ions about a n.n. complex. They propose for KCl containing Ca^{2+} or Sr^{2+} that two of the six nearest chloride ions undergo nonradial displacements about the impurity ion. The displacements are shown in Fig. 1. The nonradial displacements are the vector sum of ϵ_I and ϵ_V, where ϵ_I is due to the extra positive charge of the divalent ion, and ϵ_V is due to the missing positive charge at the site of the vacancy. In NaCl these displacements were calculated to be somewhat smaller. Bassani and Fumi's model considers the cation impurity, the center of effective vacancy charge,[7] and all lattice ions but the n.n. halide ions, to remain at the normal lattice sites. The treatment presented in this paper includes the possibility that the cation impurity and vacancy are displaced toward each other as a result of Coulomb attraction. These displacements are shown as Δ_I and Δ_V in Fig. 1. Since the Sm^{2+} ion has the same charge and a similar size to that of Ca^{2+} and Sr^{2+}, one of the points of interest of the present work was whether the predicted nonradial displacements could be detected by optical spectroscopy.

The ionic displacements can be calculated through the usual theory of crystal-field (c.f.) effects on elec-

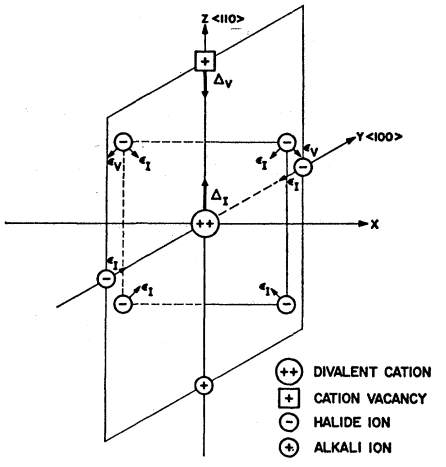

FIG. 1. Defect complex consisting of the divalent cation impurity, the cation vacancy, and six nearest-neighbor halide ions. Possible displacements from normal lattice positions are shown as ϵ_I, ϵ_V, Δ_I, and Δ_V.

* Present address: IBM San Jose Research Laboratory, San Jose, California.

[1] F. Bassani and F. G. Fumi, Nuovo Cimento **11**, 274 (1954).
[2] G. D. Watkins, Phys. Rev. **113**, 79 (1959); **113**, 91 (1959).
[3] Y. Haven, J. Chem. Phys. **21**, 171 (1953).
[4] J. Dryden and R. Meakins, Discussion Faraday Soc. **23**, 39 (1957).
[5] R. W. Dreyfus, Phys. Rev. **121**, 1675 (1961).
[6] R. W. Dreyfus and R. B. Laibowitz, Phys. Rev. **135** A1413 (1964).

[7] For simplicity, a displacement in the center of effective vacancy charge is hereafter referred to as simply a change in the "position" of the vacancy.

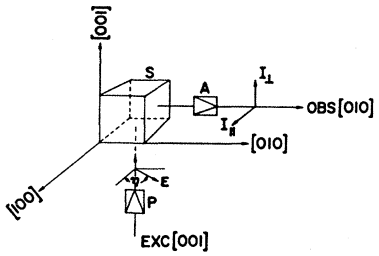

FIG. 2. Experimental arrangement for the determination of polarized emission under polarized excitation.

tronic spectra. The crystal-field potential due to a distribution of ions about a central ion contributes to the total Hamiltonian of the central ion a term

$$H_{c.f.}=-e\sum_i V(r_i,\theta_i,\psi_i)\,,$$

where the sum extends over all the electrons of the ion. It is usual to expand this term in a series of spherical harmonics

$$H_{c.f.}=\sum_{i,\mu,\nu} A_\nu^\mu r_i^\nu Y_\nu^\mu(\theta_i,\phi_i)\,. \tag{1}$$

When $H_{c.f.}$ is small, it may be treated as a first-order perturbation which yields a crystal-field splitting of the free-ion spectral lines. The matrix element of the perturbation is then

$$\langle\Psi|H_{c.f.}|\Psi'\rangle=B_\nu^\mu\langle\psi|Y_\nu^\mu|\psi'\rangle\,, \tag{2}$$

where

$$B_\nu^\mu=\langle r^\nu\rangle A_\nu^\mu \tag{3}$$

and ψ and ψ' denote the angular part of the wave function. In this paper the crystal-field interaction is considered to act only within individual degenerate free-ion states of given S, L, and J of the Sm^{2+} ion. Only the even-order matrix elements need, therefore, be considered. Using the Wigner-Eckart theorem, these matrix elements can be written[8]

$$\langle f^6\alpha SLJM|Y_\nu^\mu|f^6\alpha SLJM'\rangle = C^{J\nu J}_{M\mu M'}(\alpha SLJ\|Y_\nu\|\alpha SLJ)\,, \tag{4}$$

where f^6 specifies the configuration, S, L, J, M have their usual meaning, and α represents all other quantum numbers. The C's are Wigner coefficients and $(\alpha SLJ\|Y_\nu\|\alpha SLJ)$ are reduced matrix elements. Alternatively, it is possible to calculate the matrix elements from the general tensor-operator methods developed by Racah. Following Judd[9]

$$\langle f^6\alpha SLJM|U_\mu^\nu|f^6\alpha SLJM'\rangle=(-1)^{J-M}\begin{pmatrix} J\nu J \\ -M\mu M'\end{pmatrix} \times(-1)^{S+\nu+J+L}[2J+1]\times\begin{Bmatrix} LJS \\ J L\nu\end{Bmatrix}(\psi\|U^\nu\|\psi)\,, \tag{5}$$

where $(\psi\|U^\nu\|\psi)$ is a "doubly reduced" matrix element related to the reduced matrix element of Eq. (4). (U^ν is a spherical tensor operator defined in detail in Ref. 9.)

[8] J. L. Prather, Natl. Bur. Std. (U.S.) Monograph **19** (1961).
[9] B. R. Judd, *Operator Techniques in Atomic Spectroscopy* (McGraw-Hill Book Company, Inc., New York, 1963).

The coefficients B_ν^μ of Eqs. (2) and (3) can be treated as experimental parameters to be obtained from the observed crystal-field splitting. It is, in principle, also possible to calculate the coefficients A_ν^μ of Eqs. (1) and (3), if the location (in terms of the spherical coordinates R_j, α_j, β_j) and effective charge (q_je) of all ions about the central ion are known. In order to facilitate the calculation, the assumption is usually made that polarization of the lattice ions, as well as charge overlap and covalency effects, may be neglected. Criticism of this procedure is reserved for a later section in the discussion. Under this assumption, the A_ν^μ are

$$A_\nu^\mu=\frac{4\pi}{2\nu+1}\sum_j\frac{q_je^2}{R_j^{\nu+1}}Y^*{}_\nu^\mu(\alpha_j,\beta_j)\,, \tag{6}$$

where R_j is the distance between the jth ion and the central ion, and where the sum extends over all the ions of the lattice. For example, the crystal-field coefficients may be written in terms of the displacements proposed by Bassani and Fumi for the present lattice imperfection. A comparison with the empirical coefficients then yields values for the displacements of the ions considered.

In order to determine the matrix elements of the crystal-field perturbation by group theoretic methods, the site symmetry of the optically active ion and the crystal-field term assignments of its energy levels must be known. The number of stark components into which a free-ion level of given J is split by the crystal field gives an indication of the crystal-field symmetry. A more powerful experimental tool is the polarization of emission under linearly polarized excitation. The origin of polarized emission from anisotropic centers in cubic lattices has recently been reviewed in detail by Feofilov.[10] A fraction of the anisotropic centers which lie along crystallographically equivalent directions of the host lattice can be preferentially excited depending on the nature of the dipole moment associated with the absorbing transition. The subsequent emission from these centers is then polarized in a manner depending on the nature of the dipole moment associated with the emitting transition. The polarized emission data, therefore, specifies the transition dipole type (electric or magnetic) and its orientation. This information, together with the selection rules governing transitions between stark components, usually suffices to make crystal field term assignments.

EXPERIMENTAL METHODS

Single crystals of samarium-doped alkali halides were prepared by the Kyropolous method from mixed melts of $SmCl_2$ with either KCl, KBr, NaCl, KI, or RbCl. A modified Cary Model 14R spectrophotometer was used for the absorption and emission spectra. The modifica-

[10] P. P. Feofilov, *The Physical Basis of Polarized Emission* (Consultants Bureau, Inc., New York, 1961).

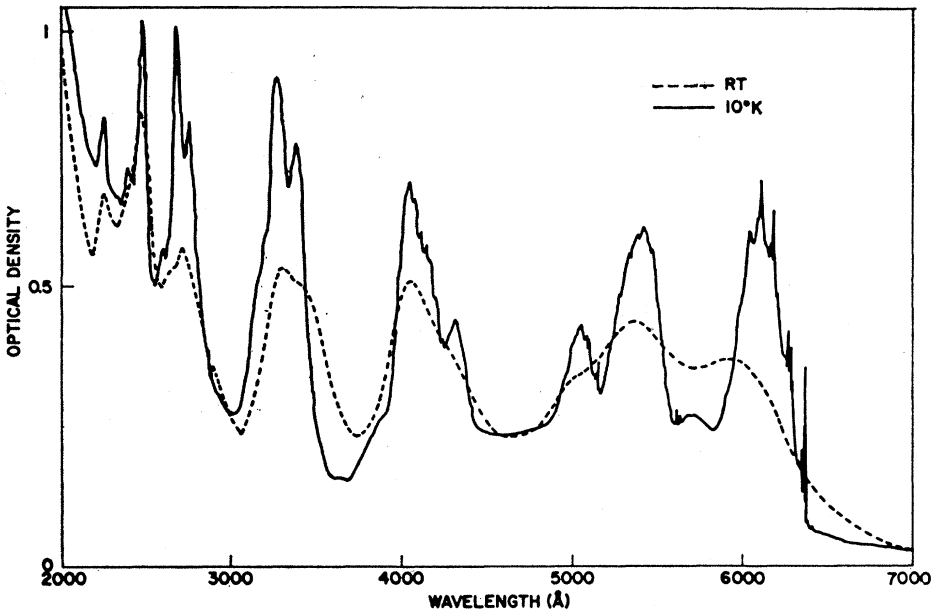

FIG. 3. Absorption spectrum of Sm^{2+}:KCl at room temperature and at 10°K.

tion was necessary in order to obtain resolution of the order of 0.5 Å in the 6500- to 7300-Å region. For this purpose an Osram high-pressure xenon lamp was substituted for the normal tungsten filament lamp and a DuMont Model K-2175 photomultiplier tube with S-20 response was substituted for the normal 1P28 photomultiplier tube. In the 7300- to 9600-Å region resolutions of from 1–4 Å were obtained through the use of a cooled Philips 150 CVP photomultiplier with a S-1 response. The lower resolution applies to wavelengths of greater than 8000 Å. Emission spectra were taken with excitation light from the xenon lamp through a $CuSO_4$ filter and either broad- or narrow-band filters which transmitted light in the region of the absorption spectra but not in the region of the emission spectra. The excitation was in a direction perpendicular to the direction of observation.

In general, it was possible to distinguish two sets of absorption and emission bands. One set was due to dispersed Sm^{2+} ions, the other to Sm^{2+} ions which are part of precipitates. The spectra due to precipitates could be entirely eliminated by quenching samples from 600°C to room temperature in air. All samples to be discussed here were treated in this way.

Polarization of the emission was also determined. The method of excitation and observation is described in terms of Fig. 2. Filtered excitation light from the xenon lamp or the 6328-Å line of a He-Ne gas laser was linearly polarized by passing it through an Ahrens prism (P). Excitation light travelling in the [001] direction of the alkali-halide crystal (S) was linearly polarized for values of the azimuthal angle (η) from 0° to 180° relative to the [100] direction of the crystal. The intensity of the emitted light in the [010] direction was measured through an analyzing Ahrens prism (A) in directions parallel ($I_{\parallel}$) and perpendicular ($I_{\perp}$) to the [100] direction of the crystal.

The degree of polarization and the intensities are functions of (η). The polarization $P(\eta)$ is defined in the usual way:

$$P(\eta)=\frac{I_{\parallel}(\eta)-I_{\perp}(\eta)}{I_{\parallel}(\eta)+I_{\perp}(\eta)}. \tag{7}$$

A number of precautions were taken to limit sources of experimental depolarization. The polarization inherent in the spectrophotometer (P_0) was calibrated using an unpolarized light source. The observed polarization from the sample (P_{obs}) was then corrected using the relationship[10]

$$P=\frac{P_{obs}-P_0}{1-P_{obs}P_0}. \tag{8}$$

The instrumentation was checked by measuring the polarized luminescence from M centers in KCl and comparing it with published data.[11,12] Samples were carefully checked for internal strains. Only samples without macroscopic strain were used. The incident and emerging optics were arranged to give better than 99% polarization. In addition, a slit system was placed between the sample and the analyzing prism so as to minimize in the emission any light which had suffered reflection at the surfaces of the sample.

EXPERIMENTAL RESULTS

I. Absorption and Emission Spectra

At room temperature and at liquid-nitrogen temperature a series of up to 20 broad absorption bands are ob-

[11] J. Lambe and W. D. Compton, Phys. Rev. **106**, 684 (1957).
[12] C. Z. van Doorn, Philips Res. Rept. **12**, 309 (1957).

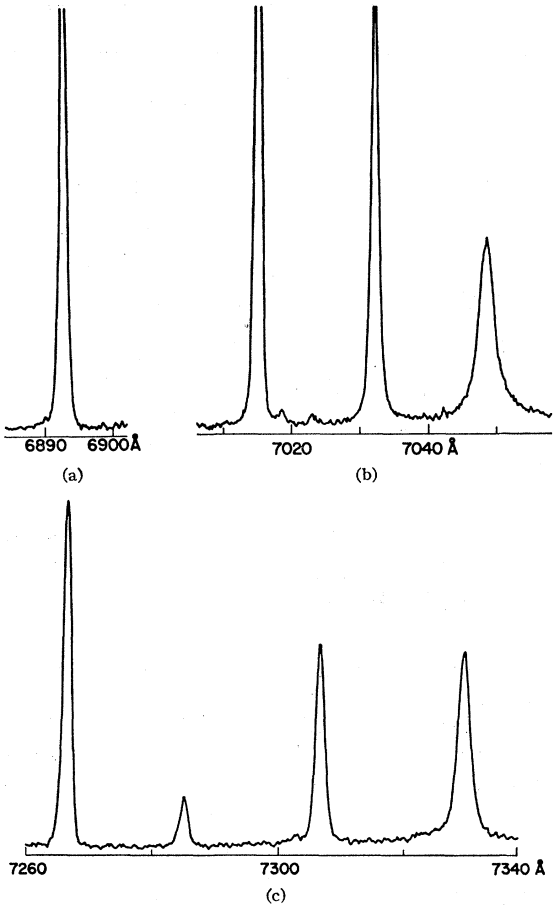

FIG. 4. First three (high-energy) sets of sharp emission lines of Sm^{2+}:KCl at 10°K.

served between 2000 and 6000 Å. A single very broad emission band is observed at these temperatures which starts at 6900 Å and persists beyond 11 000 Å. At 10°K sharp lines are observed in the absorption spectra in addition to the broad bands. The half-width of the broad bands is narrower, and their peak positions occur at lower energies than at the higher temperatures. The absorption spectrum of Sm^{2+}:KCl is shown in Fig. 3, and Table I lists the peak position of the broad bands at room temperature and at 10°K. The peak positions of the first absorption band of Sm^{2+} in RbCl, KCl, KBr, NaCl, and KI are shifted to lower energies in that order. For comparison, Table I also lists the position of the lowest energy band for these alkali halides. (The sharp absorption lines are vibronic in origin and are to be treated elsewhere, together with similar vibronic spectra observed in alkali halides containing Eu^{2+} and Yb^{2+}.)

At 10°K the high-temperature emission spectra in KCl, KBr, and RbCl are completely replaced by a number of sets of narrow lines. These lines appear in sets of Stark components; a singlet near 6890 Å, a triplet in the 7030-Å region, a quintet in the 7280-Å region, plus four more sets of lines, the last near 9500 Å. In the 8000- to 9600-Å region of the spectrum, the individual Stark components are not fully resolved. This results from the general decrease in resolution of the spectrophotometer in this region and from the inherent decrease in intensity of these lines relative to those in the 6900- to 7600-Å region. Figure 4 shows the first three sets of sharp lines observed in KCl at 10°K. In NaCl a sharp line is observed near 6893 Å and a doublet in the 7000-Å region. The remainder of the emission spectrum in NaCl consists of a number of sharp lines superimposed on a broad band which starts near 7100-Å and continues beyond 11 000 Å. In KI only the broad band emission is observed. This broad-band emission in NaCl and KI is similar to that observed in precipitated crystals of the other alkali halides. It is not clear whether the broad emission in NaCl and KI is an intrinsic property of isolated Sm^{2+} ions in these lattices or that for these crystals the quenching procedure is not able to eliminate the precipitation phase.

Table II lists all the sharp lines observed in KCl, KBr, and RbCl at 10°K. The relative integrated intensities shown in column 4 are determined relative to the most intense line within each set of Stark components. No attempt has been made to obtain the relative emission intensity between different sets of Stark components, or to correct for the angular dependence of the intensity. (The polarization data of this table are discussed in Sec. II.)

The energy level diagram shown in Fig. 5 is deduced from the absorption and emission spectra of Sm^{2+}:KCl at 10°K on the assumption that all emission transitions originate at the singlet level designated $^5D_0$. The shaded area gives the location of the lowest energy absorption

TABLE I. Peak position of broad band absorption lines.

	300°K	10°K
Sm^{2+}:KCl	16 835 cm^{-1}	16 375 cm^{-1}
		17 550
	18 622	18 464
		19 818
		23 180
	24 661	24 863
		25 806
		29 612
	29 455	
	30 257	30 544
		31 756
		36 289
	36 765	37 230
		38 256
		40 112
	40 241	41 322
	44 346	44 287
Sm^{2+}:KBr	16 722	16 340
Sm^{2+}:KI	16 181	15 886
Sm^{2+}:NaCl	16 260	15 936
Sm^{2+}:RbCl	16 736	16 529

TABLE II. Splitting and crystal field assignments of the ^7F_J multiplet for Sm^{2+} in alkali halides.

	Spectrographic data						Polarization data						
1	2	3	4	5	6	7	8	9	10	11	12	13	14
J value	Emission wavelength (Å)	Emission frequency (cm^{-1})	Relative intensity[a]	Energy level (cm^{-1})	Center of gravity[b] (cm^{-1})	Landé interval (cm^{-1})	$P(\eta)$	$I_{\parallel}(\eta)$	$I_{\perp}(\eta)$	Absorption dipole	Emission dipole	c.f. term from polarization	Final c.f. term assignment
							(a) KCl						
0	6 892.8	14 507.9	10.0	0	0	0	$-f(\cos\eta)$[d]	$\sin^2\eta$[d]	const[d]		Z_e, X_e	A_1, B_1	A_1
	7 015.6	14 253.9	10.0	254.0			-1	const	$\cos^2\eta$		Y_m	B_1	B_1
1	7 032.6	14 219.5	8.8	288.4	288.1	288.1	$+f(\cos\eta)$	const	$\sin^2\eta$		Z_m, X_m	A_2, B_2	B_2
	7 049.2	14 186.0	7.1	321.9			$+f(\cos\eta)$	const	$\sin^2\eta$		Z_m, X_m	A_2, B_2	A_2
	7 266.5	13 761.8	10.0	746.1			$-f(\cos\eta)$	$\sin^2\eta$	const		Z_e, X_e	A_1, B_1	A_1
	7 266.5[c]	13 761.7		746.2						Y_e			A_1'
2	7 285.0	13 726.8	1.6	781.2	792.0	252.0	$-f(\cos\eta)$	const	$\sin^2\eta$		Z_m, X_m	A_2, B_2	A_2
	7 306.8	13 685.9	6.5	822.0			$+1$	$\cos^2\eta$	const		Y_e	B_2	B_2
	7 329.6	13 643.3	9.5	864.6			$-f(\cos\eta)$	$\sin^2\eta$	const		Z_e, X_e	A_1, B_1	B_1
	7 663.8	13 048.4	0.1	1 459.5									
	7 668.6	13 040.2	0.1	1 467.7									
3	7 670.1	13 037.6	0.2	1 470.3	1 481.1	230.0							
	7 673.8	13 031.4	0.5	1 476.5									
	7 686.9	13 009.1	0.2	1 498.8									
	7 695.9	12 993.9	10.0	1 514.0			$-f(\cos\eta)$	$\sin^2\eta$	const		Z_e, X_e	A_1, B_1	A_1 or B_1
	8 134.0	12 294.1	0.7	2 218.8									
4	8 195.9	12 201.2	3.5	2 306.7	2 282.6	200.4	$-f(\cos\eta)$	$\sin^2\eta$	const		Z_e, X_e	A_1, B_1	A_1 or B_1
	8 206.4	12 185.6	10.0	2 322.3			$-f(\cos\eta)$	$\sin^2\eta$	const		Z_e, X_e	A_1, B_1	A_1 or B_1
	8 749.5	11 429.0	3.6	3 078.9									
	8 769.1	11 403.7	0.1	3 104.2									
5	8 781.1	11 388.1	7.3	3 119.9	3 149.3	173.3	$-f(\cos\eta)$	$\sin^2\eta$	const		Z_e, X_e	A_1, B_1	A_1 or B_1
	8 834.2	11 319.6	10.0	3 188.3			$+1$	$\cos^2\eta$	const		Y_e	B_2	B_2
	8 842.2	11 309.4	0.9	3 198.5									
	8 848.0	11 302.0	7.6	3 205.9									
	9 442.2	10 509.8	10.0	3 917.1			$-f(\cos\eta)$	$\sin^2\eta$	const		Z_e, X_e	A_1, B_1	A_1 or B_1
	9 506.0	10 519.7	0.6	3 988.2									
6	9 517.9	10 506.5	0.7	4 001.4	3 979.0	138.3							
	9 525.9	10 497.7	0.5	4 010.2									
							(b) KBr						
0	6 891.0	14 511.7	10.0	0	0		$+f(\cos\eta)$[d]	$\cos^2\eta$[d]	const[d]		Z_e, X_e	A_1, B_1	A_1
	7 016.4	14 252.3	10.0	259.4			$+f(\cos\eta)$	const	$\sin^2\eta$		Y_m	B_1	B_1
1	7 032.6	14 219.5	8.7	292.2	288.9	288.9	$-f(\cos\eta)$	const	$\cos^2\eta$		Z_m, X_m	B_2, A_2	B_2
	7 044.0	14 196.5	9.2	315.2			$-f(\cos\eta)$	const	$\cos^2\eta$		Z_m, X_m	B_2, A_2	A_2
	7 271.8	13 751.8	5.2	759.9			$+f(\cos\eta)$	$\cos^2\eta$	const		Z_e, X_e	A_1, B_1	A_1
	7 271.8[c]	13 751.7		760.0									A_1'
2	7 288.1	13 721.0	3.4	790.7	795.8	253.5							A_2
	7 302.1	13 694.7	7.0	817.0			$-f(\cos\eta)$	$\sin^2\eta$	const		Y_e	B_2	B_2
	7 320.6	13 660.1	10.0	851.6			$+f(\cos\eta)$	$\cos^2\eta$	const		Z_e, X_e	A_1, B_1	B_1
	7 667.5	13 042.1	0.1	1 469.6						Z_e			
	7 671.6	13 035.1	0.3	1 476.6									
3	7 679.6	13 021.5	0.2	1 490.2	1 488.9	231.0				or			
	7 686.7	13 009.5	10.0	1 502.2			$+f(\cos\eta)$	$\cos^2\eta$	const		Z_e, X_e	A_1, B_1	A_1 or B_1
	7 689.0	13 005.6	2.3	1 506.1						X_e			
	8 141.5	12 282.7	1.0	2 229.0			$+f(\cos\eta)$	$\cos^2\eta$	const		Z_e, X_e	A_1, B_1	A_1 or B_1
4	8 187.7	12 213.4	6.8	2 298.3	2 278.6	197.4							
	8 194.6	12 203.2	10.0	2 308.5			$+f(\cos\eta)$	$\cos^2\eta$	const		Z_e, X_e	A_1, B_1	A_1 or B_1
	8 755.8	11 421.0	1.8	3 090.7									
	8 769.3	11 403.4	1.0	3 108.3			$+f(\cos\eta)$	$\cos^2\eta$	const		Z_e, X_e	A_1, B_1	A_1 or B_1
	8 781.1	11 388.1	6.6	3 123.6									
5	8 820.1	11 337.7	10.0	3 174.0	3 144.8	173.2							
	8 827.0	11 328.9		3 182.8									
	8 832.0	11 322.5	10.0	3 189.2									
	9 456.0	10 575.3	10.0	3 936.4			$+f(\cos\eta)$	$\cos^2\eta$	const		Z_e, X_e	A_1, B_1	A_1 or B_1
	9 514.0	10 510.5	0.9	4 001.2									
6	9 522.0	10 502.0	2.0	4 009.7	3 991.3	141.1							
	9 529.3	10 494.0	0.4	4 017.7									

TABLE II (*continued*)

	Spectrographic data						Polarization data						
1	2	3	4	5	6	7	8	9	10	11	12	13	14
J value	Emission wavelength (Å)	Emission frequency (cm^{-1})	Relative intensity[a]	Energy level (cm^{-1})	Center of gravity[b] (cm^{-1})	Landé interval (cm^{-1})	$P(\eta)$	$I_{\parallel}(\eta)$	$I_{\perp}(\eta)$	Absorption dipole	Emission dipole	c.f. term from polarization	Final c.f. term assignment
						(c) RbCl							
0	6 886.4	14 521.4	10.0	0	0	0	$-f(\cos\eta)$[d]	$\sin^2\eta$[d]	const[d]		Z_e, X_e	A_1, B_1	A_1
	7 009.6	14 266.1	10.0	255.3			$-f(\cos\eta)$	const	$\cos^2\eta$		Y_m	B_1	B_1
1	7 025.5	14 233.9	7.3	287.5	287.6	287.6	$+f(\cos\eta)$	const	$\sin^2\eta$		Z_m, X_m	A_2, B_2	B_2
	7 041.6	14 201.3	4.9	320.1			$+f(\cos\eta)$	const	$\sin^2\eta$		Z_m, X_m	A_2, B_2	A_2
	7 258.6	13 776.7	1.2	745.5						Y_e			A_1
	7 259.9	13 774.3	10.0	747.1			$-f(\cos\eta)$	$\sin^2\eta$	const		Z_e, X_e	A_1, B_1	A_1
2	7 277.5	13 741.0	1.5	780.4	791.0	251.7							A_2
	7 298.5	13 700.9	4.4	820.5			$+f(\cos\eta)$	$\cos^2\eta$	const		Y_e	B_2	B_2
	7 320.5	13 659.9	1.4	861.5			$-f(\cos\eta)$	$\sin^2\eta$	const		Z_e, X_e	A_1, B_1	B_1
	7 658.5	13 057.4	0.1	1 464.0									
	7 663.5	13 048.7	0.4	1 472.7									
3	7 675.6	13 028.3	0.4	1 493.1	1 492.5	233.8							
	7 684.5	13 013.2	10.0	1 508.2									
	7 694.0	12 997.1	0.2	1 524.3									
	8 183.8	12 219.3	1.7	2 302.1									
4	8 192.4	12 206.4	5.8	2 315.0	2 311.3	203.8							
	8 193.7	12 204.5	10.0	2 316.9									
	8 737.3	11 445.2	2.3	3 076.2									
	8 757.5	11 418.8	1.4	3 102.6									
5	8 768.0	11 405.1	6.2	3 116.3	3 134.7	164.7							
	8 818.6	11 339.7	10.0	3 181.7									
	8 830.3	11 324.6	7.7	3 196.8									
	9 431.3	10 603.1	10.0	3 918.3									
6	9 492.0	10 535.2	1.0	3 986.2	3 976.9	140.4							
	9 503.0	10 523.0	2.4	3 998.4									
	9 509.0	10 516.4	0.9	4 005.0									

[a] Integrated intensity relative to the most intense Stark component of a set of levels with same J.
[b] For $J>2$ the values of the center of gravity are only approximate.
[c] This line not observed; obtained from computer best fit analysis.
[d] Because of the inherent depolarization, the predicted dependence on $\cos^2\eta$ was not observed. The observed $P(\eta)$ does depend on some $f(\cos\eta)$ as can be seen from Fig. 6. Similarly, the dependence of $I_{\parallel}$ and $I_{\perp}$ on η was proportional to the one indicated.

band which is most likely due to a transition from the $4f^6$ ground configuration to the excited $4f^5 5d$ configuration. The free-ion term assignments given in column 1 of Table II are made by comparison with assignments by Dieke and Sarup[13] in $LaCl_3$ and by others for Sm^{2+} and Eu^{3+} in other host lattices for the transitions within the $4f^6$ configuration.[14–17] Energies for the ^7F multiplet and the $^5D_0$ level of Sm^{2+} in the alkali halides correspond very well with the values reported for other crystals.

An uncertainty exists as to whether the levels designated as $^5D_1$ are indeed due to electronic transitions within the $4f^6$ configuration, or are due to transitions to one of a set of vibronic levels associated with transitions to the $4f^5 5d$ configuration. These levels are, therefore, shown as dashed lines in Fig. 5 to indicate this uncertainty. Emission from these levels was not observed.

Russell-Saunders coupling is not strictly obeyed within the ground ^7F multiplet. It may be seen from column 7 of Table II that the approximate[18] Lande interval decreases with higher J values. Similar results may be obtained from the data of Dieke and Sarup[13] and of Wood and Kaiser.[14]

II. Polarization of Emission

Polarized emission resulting from linearly polarized excitation was studied by the method described earlier. No polarized emission was observed with polarized excitation of 90-Å band width centered about the peak wavelengths of either of the three lowest energy absorption bands. A likely explanation of this result is that the

[13] G. H. Dieke and R. Sarup, J. Chem. Phys. **36**, 371 (1962).
[14] D. L. Wood and W. Kaiser, Phys. Rev. **126**, 2079 (1962).
[15] P. P. Feofilov and A. A. Kaplyanski, Opt. i Spektroskopiya **12**, 493 (1962) [English transl.: Soviet Phys.—Opt. Spectry. **12**, 272 (1962)].
[16] J. D. Kingsley and J. S. Prener, Phys. Rev. **126**, 458 (1962).
[17] L. G. DeShazer and G. H. Dieke, J. Chem. Phys. **38**, 2190 (1963).

[18] The values of column 7 of Table II were obtained by taking the center of gravity (column 6) of all observed lines in each set. Since for $J>2$ not all possible lines are observed, the values given are only approximate, but sufficiently correct to show the trend in the Lande interval.

broad absorption bands contain a number of closely spaced energy levels. These levels originate from weakly split $4f^5$ core states, or are vibronic states. If these states have different crystal-field representations, then more than one type of absorption dipole can be simultaneously excited. The effective excitation may, therefore, be unpolarized. This hypothesis was checked by exciting the sample with a monochromatic polarized excitation source. A convenient source was found to be the 6328-Å line of the He-Ne gas laser, which overlaps the low-energy side of the first broad absorption band. The resultant emission was polarized.

Figure 6 shows a typical result for $P(\eta)$, $I_{\parallel}(\eta)$, and $I_{\perp}(\eta)$. These values are tabulated in columns 8, 9, and 10 of Table II for a number of emission lines. As a result of apparatus limitations, only the polarization of the most intense lines could be obtained for levels of $J>2$.

DISCUSSION OF RESULTS

Calculation of the crystal-field coefficients B_ν^μ from the experimental data involves a number of steps, some of which require a brief discussion. Crystal-field term assignments are first made using the results of the polarization experiment. The matrix elements are calculated next from previously symmetrized wave functions. The coefficients B_2^μ and B_4^μ were then calculated from the observed splitting of $^7F_1$ and $^7F_2$ states.[19] Since some ambiguity exists in the term assignments based on the polarization results (see column 13, Table II), and since the location of one of the Stark components of the $^7F_2$ level is not observed in Sm^{2+}:KCl and KBr, a numerical analysis of the data was used to obtain the c.f. coefficients.

In addition, the coefficients A_ν^μ were calculated for two point-charge models of the ions surrounding the Sm^{2+} ion. Finally, the experimentally obtained coefficients and those calculated from the point-charge models were compared.

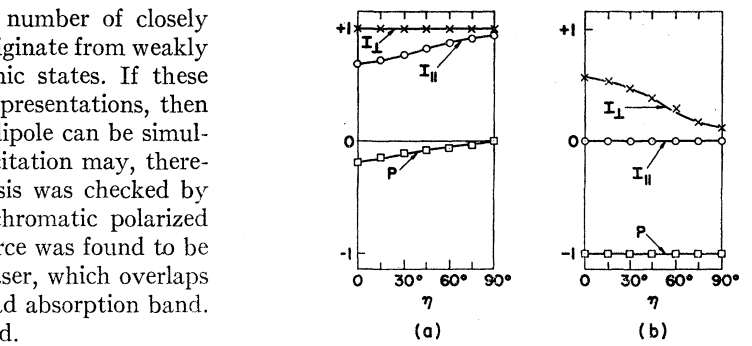

FIG. 6. Typical polarized emission data shown as a function of the azimuthal angle (η). The data is from (a) the 6892.8-Å line, and (b) the 7016.5-Å line of Sm^{2+}:KCl at 10°K.

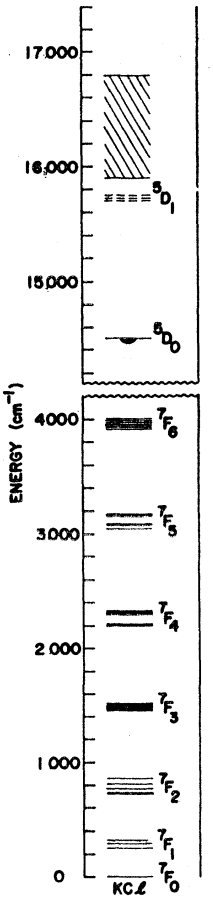

FIG. 5. Energy level diagram derived from absorption and emission spectra of Sm^{2+}:KCl at 10°K.

I. Identification of Site Symmetry and Crystal-Field Assignments

Classically one of the transition dipole moments of an anisotropic center is considered to be oriented along the symmetry axis (Z axis) of the center. An optical transition which excites this dipole is either an electric dipole (Z_e) or a magnetic dipole (Z_m),[20] or higher order pole transition. It is possible to describe two additional, mutually perpendicular, dipole moments which lie in the XY plane. If the symmetry is greater than twofold rotational symmetry (C_2), then it is possible to combine these dipoles into electric (XY_e) or magnetic (XY_m) rotors.[21] This is so because linear combinations of X and Y form a basis for irreducible representations of the symmetry group. For less than threefold rotational symmetry (C_3), as is the case for the Sm^{2+}-vacancy center, a rotor cannot be defined. Instead, three mutually inequivalent dipoles exist which lie along the Z, X, and Y direction.

In the past, polarization data have been analyzed in terms of rotors even for cases of less than C_3 sym-

[19] As mentioned earlier, the data for $J>2$ are incomplete. In the discussion of the results which follows, only the data from the $^7F_1$ and $^7F_2$ states are considered.

[20] π_e or π_m in Feofilov's notation.

[21] σ_e or σ_m in Feofilov's notation.

TABLE III. Polarized emission from C_2 center along various axes.

(a) ⟨110⟩

Absorption \ Emission		Z_e or X_e	Y_e	Z_m or X_m	Y_m
Z_e or X_e	P	$\frac{\cos^2\eta}{2+\cos^2\eta}$	$-\frac{\cos^2\eta}{2-\cos^2\eta}$	$-\frac{\cos^2\eta}{2+\cos^2\eta}$	$\frac{\cos^2\eta}{2-\cos^2\eta}$
	$I_\parallel$	$\frac{1}{2}(1+\cos^2\eta)$	$\sin^2\eta$	$\frac{1}{2}$	1
	$I_\perp$	$\frac{1}{2}$	1	$\frac{1}{2}(1+\cos^2\eta)$	$\sin^2\eta$
Y_e	P	$-\frac{\cos^2\eta}{2-\cos^2\eta}$	1	$\frac{\cos^2\eta}{2-\cos^2\eta}$	-1
	$I_\parallel$	$\sin^2\eta$	$\cos^2\eta$	1	0
	$I_\perp$	1	0	$\sin^2\eta$	$\cos^2\eta$

(b) ⟨100⟩

Absorption \ Emission		Z_e	X_e	Y_e	Z_m	X_m	Y_m
Z_e	P	1	-1	$-\cos^2\eta$	-1	1	$\cos^2\eta$
	$I_\parallel$	$\cos^2\eta$	0	$\sin^2\eta$	0	$\sin^2\eta$	$\cos^2\eta$
	$I_\perp$	0	$\sin^2\eta$	$\cos^2\eta$	$\cos^2\eta$	0	$\sin^2\eta$
X_e	P	$-\cos^2\eta$	1	-1	$\cos^2\eta$	-1	1
	$I_\parallel$	$\sin^2\eta$	$\cos^2\eta$	0	$\cos^2\eta$	0	$\sin^2\eta$
	$I_\perp$	$\cos^2\eta$	0	$\sin^2\eta$	$\sin^2\eta$	$\cos^2\eta$	0
Y_e	P	-1	$-\cos^2\eta$	1	1	$\cos^2\eta$	-1
	$I_\parallel$	0	$\sin^2\eta$	$\cos^2\eta$	$\sin^2\eta$	$\cos^2\eta$	0
	$I_\perp$	$\sin^2\eta$	$\cos^2\eta$	0	0	$\sin^2\eta$	$\cos^2\eta$

(c) ⟨100⟩

Absorption \ Emission		Z_e	XY_e	Z_m	XY_m
Z_e	P	1	$-\frac{\cos^2\eta}{2-\cos^2\eta}$	-1	$\frac{\cos^2\eta}{2-\cos^2\eta}$
	$I_\parallel$	$\cos^2\eta$	$\sin^2\eta$	0	1
	$I_\perp$	0	1	$\cos^2\eta$	$\sin^2\eta$
XY_e	P	$-\frac{\cos^2\eta}{2-\cos^2\eta}$	$\frac{\cos^2\eta}{2+\cos^2\eta}$	$\frac{\cos^2\eta}{2-\cos^2\eta}$	$-\frac{\cos^2\eta}{2+\cos^2\eta}$
	$I_\parallel$	$\sin^2\eta$	$\cos^2\eta+1$	1	1
	$I_\perp$	1	1	$\sin^2\eta$	$\cos^2\eta+1$

metry.[10,22] Conclusions based on this procedure may be incorrect, since if it is used it predicts polarized emission from a C_2 center which, in most cases, is indistinguishable from one having a fourfold rotational axis (C_4). On the other hand, if three inequivalent transition dipole moments are used these symmetries can be distinguished, as is shown below.

An analysis of $P(\eta)$, $I_\parallel(\eta)$, $I_\perp(\eta)$ for a C_2 center, with a Z axis along a ⟨110⟩ direction of the alkali-halide lattice, has been carried out in terms of three inequivalent transition dipole moments. The results are given in Table III(a). For comparison Table III(b) and Table III(c) give the predicted polarization for C_2 and C_4 centers with Z axis lying along a ⟨100⟩ direction. Since in the present experiment the absorption transitions are strong and undoubtedly between configurations of opposite parity, only absorbing transitions involving electric dipole moments are tabulated.

It should be pointed out that the empirical $P(\eta)$, $I_\parallel(\eta)$, and $I_\perp(\eta)$ differed in magnitude from the predicted values. The difference is the result of depolarization which, in view of the precautions taken to minimize experimental depolarization, must be considered to be in part an inherent property of the emission. Such depolarization effects are, in fact, normally observed (see, e.g., Ref. 22). Although the magnitude of the polarization parameters are changed, the functional relationship with η is not. It is on the basis of this relationship that the polarization data are analyzed.

The experimental fact that for some lines the degree of polarization is not a function of η, i.e., is equal to ± 1 [see, e.g., the 7015.6- and 7306.8 Å lines in Table II(a)] eliminates the possibility that the absorption involves a XY_e rotor in a C_4 center. It is possible to exclude absorption involving a Z_e dipole in a C_4 center or a C_2 center along a ⟨100⟩ direction of the lattice in the following way. The transition $^5D_0 \rightarrow {}^7F_0$ involves two $J=0$ levels. In the three types of symmetries both levels belong to the A_1 c.f. representation and the transition between them, which yields the 6890-Å emission line, is required to go via a Z_e dipole moment. Comparison of the observed $P(\eta)$, $I_\parallel(\eta)$, and $I_\perp(\eta)$ for this line in, e.g., Sm^{2+}:KCl and the predicted values shows that the results are compatible only if: (1) the center has an axis of C_2 symmetry along a ⟨110⟩ direction, and (2) that absorption involves a Y_e dipole moment and emission a Z_e dipole moment. This method establishes simultaneously the symmetry, orientation, and the nature of the dipole moment associated with the absorption transition in any one alkali halide. For excitation at 6328 Å, absorption was observed to be associated with a Y_e dipole moment in Sm^{2+}:KCl and RbCl, and a Z_e (or X_e) dipole moment in Sm^{2+}:KBr (column 11, Table II). Once the absorber is known, the emission dipole moment can be established for the remaining lines from Table III. The dipole moments associated with the various emission lines are given in column 12, Table II.

Crystal-field-term assignments are made with reference to Table IV. This table lists the dipole moments associated with nonvanishing transitions between an A_1 state and all other possible terminal states for C_{2v} symmetry. (Only the A_1 emitting state is listed in Table IV, since all emission originates from the $^5D_0$ level.) Re-

TABLE IV. Selection rules for C_{2v} symmetry.

C.f. term assignment of →	Initial state	Final state			
	A_1	B_2	B_1	A_2	A_1
Transition dipole moment		Y_e, Y_m	X_e, Y_m	Z_m	Z_e

[22] S. G. Zazubovich, N. E. Lushick, and Ch. B. Lushick, Opt. i Spektroskopiya **15**, 381 (1963) [English transl.: Soviet Phys. —Opt. Spectry. **15**, 203 (1963)].

TABLE V. Basis functions within a J manifold for the C_{2v} group.

A_1	J even	ψ^0, $2^{-\frac{1}{2}}(\psi^{2k}+\psi^{-2k})$	$2k\leq J\neq 0$
	J odd	$2^{-\frac{1}{2}}(\psi^{2k}-\psi^{-2k})$	$2k\leq J-1\neq 1$
A_2	J even	$2^{-\frac{1}{2}}(\psi^{2k}-\psi^{-2k})$	$2k\leq J\neq 0$
	J odd	ψ^0, $2^{-\frac{1}{2}}(\psi^{2k}+\psi^{-2k})$	$2k\leq J-1\neq 1$
B_1	J even	$2^{-\frac{1}{2}}(\psi^{k}-\psi^{-k})$	$k\leq J-1\neq 0$
	J odd	$2^{-\frac{1}{2}}(\psi^{k}+\psi^{-k})$	$k\leq J$
B_2	J even	$2^{-\frac{1}{2}}(\psi^{k}+\psi^{-k})$	$k\leq J-1\neq 0$
	J odd	$2^{-\frac{1}{2}}(\psi^{k}-\psi^{-k})$	$k\leq J$

sulting term assignments are given in column 13, Table II.

Before discussing in detail the calculation of the crystal field, it is worth noting that qualitative information may be obtained from the number of Stark components into which a free-ion level of given J is split. For example, a free-ion state of $J=1$ should be split into three Stark components (A_2,B_1,B_2) in a field of general C_{2v} symmetry. A special C_{2v} symmetry can be defined for the present case if the displacements ϵ_I, ϵ_V, Δ_I, and Δ_V shown in Fig. 1 approach zero. In this event the c.f. coefficients $A_2^{\pm 2}$ go to zero, although they are finite for the general C_{2v} symmetry. Consequently, the $J=1$ state is split into only two Stark components (A_2,E). The observation of three Stark components for the $^7F_1$ level indicates qualitatively that the nonradial displacements of the halide ions do, indeed, occur. For the general C_{2v} symmetry a $J=2$ free-ion state should be split into 5 Stark components. Experimentally five lines were observed in Sm^{2+}:RbCl, but only four were observed in Sm^{2+}:KCl and Sm^{2+}:KBr. A computer analysis, to be discussed in detail later, of the c.f. coefficients shows, however, that an accidental degeneracy exists between the two A_1 levels of that state in Sm^{2+}:KCl and in Sm^{2+}:KBr. The missing line can be observed in a sample of Sm^{2+}:KCl containing a small amount of KBr. In this sample and in Sm^{2+}:RbCl the fifth line has approximately 0.05 integrated intensity relative to the strongest component.

II. Determination of Empirical Crystal-Field Coefficients

Crystal-field matrix elements were calculated as follows. Properly symmetrized basis functions were obtained for the C_{2v} group using zero-order wave functions and Wigner's rule.[23] Since the C_{2v} group is Abelian, the symmetrized basis functions have a simple form and can be easily expressed for all values of J as shown in Table V. The functions $\psi_\nu^{\pm\mu}$ of Table V are Legendre functions with ν equal to J. Matrix elements for the second- and fourth-order c.f. potential terms were calculated using the method of Prather[7] [Eq. (4)] and checked by using the method of Judd[9] [Eq. (5)]. It

[23] E. P. Wigner, *Group Theory* (Academic Press Inc., New York, 1959).

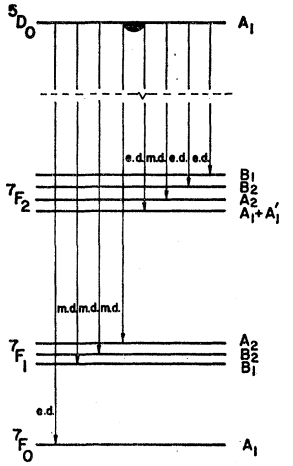

FIG. 7. Crystal-field term assignments and type of dipoles associated with the transitions $^5D_0 \rightarrow {}^7F_{0,1,2}$ in Sm^{2+}:KCl.

should be pointed out that the reduced matrix element $(\alpha 2\|Y_2\|\alpha 2)$ given by Prather is too small by a factor of 10. Correct values for the pertinent matrix elements are

$$(\alpha 1\|Y_2\|\alpha 1)=-0.199469,$$
$$(\alpha 2\|Y_2\|\alpha 2)=-0.12363,$$
$$(\alpha 2\|Y_4\|\alpha 2)=-0.150786.$$

Crystal-field coefficients were calculated through a computer fit of the experimental c.f. splittings. The program was designed to accomplish the following: (1) Allow for the uncertainty which exists in the c.f. term assignments, based on the polarization results, by permuting all ambiguous assignments, (2) account for the missing line in the $J=2$ manifold by assigning to it trial locations within a span which exceeded twice the splitting of the observed lines, (3) perform the matrix diagonalization of the two A_1 states of $J=2$, (4) determine the c.f. splitting and c.f. matrix elements for each assignment, and (5) calculate the sum of the squared deviations of the calculated splittings from the observed ones. A sharp minimum in the deviation was obtained for each alkali halide at which the value of the sum of the squared deviations was of the order of 10^{-2}. At the minimum the center of gravity of the $J=2$ manifold was 792.0 cm^{-1} for Sm^{2+}:KCl, 795.8 cm^{-1} for Sm^{2+}:KBr, and 791.0 cm^{-1} for Sm^{2+}:RbCl. Crystal-field-term assignments so obtained are given in column 14, Table II, and the location of the missing line is indicated in columns 2 and 3. Figure 7 summarizes the c.f. assignments obtained in this way, and indicates the type of dipole associated with the transitions.

TABLE VI. Empirical crystal-field coefficients (in cm^{-1}).

	KCl	RbCl	KBr
B_2^0	268.2	257.1	200.2
$B_2^{\pm 2}$	$\pm$111.5	$\pm$104.0	$\pm$103.3
B_4^0	789.5	772.2	600.6
$B_4^{\pm 2}$	$\mp$144.2	$\mp$142.5	$\mp$109.5
$B_4^{\pm 4}$	155.5	149.4	137.2

TABLE VII. Comparison of crystal-field coefficients.

	Empirical coefficients			Calculated coefficients		
				Halide displacements		Large Sm and vacancy displacements $\Delta_V=0.4a$, $\Delta_I=0.5a$
				$\epsilon_V=0.086a$ $\epsilon_I=0.141a$	$\epsilon_V=0.3a$ $\epsilon_I=0.3a$	
	KCl	RbCl	KBr	I(a)	I(b)	II
A_2^0/A_2^2	2.32	2.47	1.94	−0.31	−0.47	+8.2
A_4^0/A_4^4	5.08	5.17	4.38	−0.53	−0.87	+2.3
A_4^2/A_4^4	−0.93	−0.95	−0.80	+1.60	+76.0	−0.28

The c.f. coefficients are tabulated in Table VI. An ambiguity exists in the sign of B_2^2 and B_4^2 which arises from the c.f. diagonalization. A correlation, however, exists in the sign of these two coefficients as indicated in the table.

III. Crystal-Field Coefficients Calculated from Point-Charge Models

Comparison of the empirical c.f. coefficients to those calculated from point charge models is made in Table VII. Ratios of the coefficients are used to avoid determining $\langle r^\nu \rangle$, to minimize the effects of polarization of the lattice in the vicinity of the defect, and the effect of shielding by the $5s$ and $5p$ electrons on the $4f$ electrons of the Sm^{2+} ion.

The A_ν^μ c.f. coefficients were calculated from Eq. (6) for two point-charge models of the ion displacements around the impurity-vacancy complex. One model (Ia) is based on the displacements suggested by Bassani and Fumi. These displacements are shown as ϵ_I and ϵ_V in Fig. 1, and have been discussed in the Introduction of this paper. Bassani and Fumi obtained $\epsilon_I=0.141a$ and $\epsilon_V=0.081a$ for Ca^{2+}:KCl, where a is the n.n. distance between anions and cations in the undisplaced lattice. These displacements are sufficiently small so that the positions of all ions can be expressed as a Taylor series expansion about the normal lattice positions. The resultant c.f. coefficients are given in Table VIII as the sum of terms due to the nonradial displacement of the n.n. halide ions, the cation vacancy, and the rest of the lattice[24] corrected for the radial displacement of the n.n. halide ions. In this table $f_V=\epsilon_V/a$ and $f_I=\epsilon_I/a$. The contribution to the lattice term is primarily due to the six n.n. halides, the rest of the lattice contributing only $-(e^2/a^5)(\pi^{1/2}/6)(0.0789)$ to A_4^0, $(e^2/a^5)[(10\pi)^{1/2}/6]\times(0.0789)$ to A_4^2, and $(e^2/a^5)[(70\pi)^{1/2}/28](0.0789)$ to A_4^4.

TABLE VIII. Even crystal-field coefficients from model Ia.

	Contributing terms to c.f. coefficients.		
	Nonradial displacements	Vacancy	Lattice, corrected for radial displacements
A_2^0	$-\frac{f_v e^2}{a^3}6\left(\frac{\pi}{5}\right)^{1/2}[1+4f_I]$	$\frac{e^2}{a^3}\left(\frac{\pi}{10}\right)^{1/2}$	
A_2^2	$\frac{f_v e^2}{a^3}6\left(\frac{\pi}{30}\right)^{1/2}[1+4f_I]$		
A_4^0	$-\frac{f_v e^2}{a^5}\frac{5}{3}\left(\frac{\pi}{4}\right)^{1/2}[1+6f_I]$	$\frac{e^2}{a^5}\left(\frac{\pi}{72}\right)^{1/2}$	$-\frac{e^2}{a^5}\frac{\pi^{1/2}}{6}[3.5789+17.5f_I]$
A_4^2	$-\frac{f_v e^2}{a^5}\frac{1}{3}\left(\frac{5\pi}{2}\right)^{1/2}[1+6f_I]$		$\frac{e^2}{a^5}\frac{(10\pi)^{1/2}}{6}[3.5789+17.5f_I]$
A_4^4	$\frac{f_v e^2}{a^5}\frac{1}{6}\left(\frac{35\pi}{2}\right)^{1/2}[1+6f_I]$		$\frac{e^2}{a^5}\frac{(70\pi)^{1/2}}{28}[3.5789+17.5f_I]$

A calculation of the coefficients was also carried out for larger values of ϵ_I and ϵ_V (model Ib). In addition, the coefficients were determined for a model II in which the displacements of Ia are considered to be negligible compared with large displacements of the Sm^{2+} ion (Δ_I) and the vacancy (Δ_V) toward each other (see Fig. 1). For Ib and II, an expansion about the undisplaced lattice positions is not possible. Consequently, the results are stated in terms of the actual distances between the n.n. ions and the central ion. The resultant coefficients for model II are given in Table IX. The contribution of the remainder of the lattice ions has not been included. Since the lattice potential does not vary significantly for small distances along a $\langle 110 \rangle$ direction,[24] the contribution of the rest of the lattice to the A_4^μ may be taken to be those given above for Ia.

Each model is limited to two types of displacements so that a meaningful fit can be made to the three empirically obtained ratios of the coefficients. In each of the three models the sign of A_2^2 is positive regardless of the magnitude of the displacements. The correlation in the sign of A_4^2 to that of A_2^2, therefore, requires that A_4^2 be negative. Consequently, the uncertainty in the sign of A_2^2 and A_4^2 and therefore that of B_2^2 and B_4^2, indicated in Table VI, is removed. In comparing the empirical and calculated values, particular attention should be paid to the sign of A_4^2/A_4^4. Bassani and Fumi's model yields only positive values regardless of whether small halide displacements are used (model Ia) such as those proposed for Ca^{2+}:KCl, or larger values of ϵ_V and ϵ_I are used (model Ib). In fact, the ratio A_4^2/A_4^4 is not negative except when the Sm^{2+} ion is displaced as assumed in model II. Even for this case, a displacement exceeding 0.4a is required. The ratios given

[24] F. W. DeWette and B. R. A. Nijboer, Physica 24, 1105 (1958).

TABLE IX. Even crystal-field coefficients from model II.

$$A_2^0 \quad e^2\left(\frac{\pi}{5}\right)^{1/2}\left[\frac{2}{R_1^5}(2\Delta_I^2-a^2)+\frac{2}{R_2^5}\left(2\Delta_I^2+2\sqrt{2}\Delta_I a+\frac{a^2}{2}\right)+\frac{2}{R_3^5}\left(2\Delta_I^2-2\sqrt{2}\Delta_I a+\frac{a^2}{2}\right)\right]+\frac{e^2}{R_4^3}\frac{4\pi}{5}$$

$$A_2^2 \quad e^2\left(\frac{3\pi}{10}\right)^{1/2}\left[-\frac{2a^2}{R_1^5}+\frac{a^2}{R_2^5}+\frac{a^2}{R_3^5}\right]$$

$$A_4^0 \quad e^2\left(\frac{\pi}{12}\right)^{1/2}\left[\frac{2}{R_1^9}(8\Delta_I^4-24\Delta_I^2a^2+3a^4)+\frac{2}{R_2^9}\left(8\Delta_I^4+16\sqrt{2}\Delta_I^3a+12\Delta_I^2a^2-4\sqrt{2}\Delta_I a^3-\frac{13}{4}a^4\right)\right.$$
$$\left.+\frac{2}{R_3^9}\left(8\Delta_I^4-16\sqrt{2}\Delta_I^3a+12\Delta_I^2a^2+4\sqrt{2}\Delta_I a^3-\frac{13}{4}a^4\right)\right]+\frac{e^2}{R_4^5}\left(\frac{4\pi}{9}\right)^{1/2}$$

$$A_4^2 \quad \frac{e^2}{6}\left(\frac{5\pi}{2}\right)^{1/2}\left[\frac{2}{R_1^9}(-6\Delta_I^2a^2+a^4)+\frac{1}{R_2^9}(6\Delta_I^2a^2+6\sqrt{2}\Delta_I a^3+\tfrac{5}{2}a^4)+\frac{1}{R_3^9}(6\Delta_I^2a^2-6\sqrt{2}\Delta_I a^3+\tfrac{5}{2}a^4)\right]$$

$$A_4^4 \quad \frac{e^2}{12}\left(\frac{35\pi}{2}\right)^{1/2}\left[\frac{2a^4}{R_1^9}+\frac{a^4}{2R_2^9}+\frac{a^4}{2R_3^9}\right]$$

$$R_1=(\Delta_I^2+a^2)^{1/2} \qquad R_3=(\Delta_I^2+a^2-\sqrt{2}a\Delta_I)^{1/2}$$
$$R_2=(\Delta_I^2+a^2+\sqrt{2}a\Delta_I)^{1/2} \qquad R_4=\sqrt{2}a-(\Delta_I+\Delta_v)$$

in Table VII for model II give as close an agreement to the empirical values as can be obtained through the use of the two parameters alone.

The view is taken that the three point-charge models represent extremes of the real displacements. Agreement between models Ia and b and the empirical ratios is very poor, particularly as to sign. On the other hand, the relatively better agreement with model III indicates, to within the assumption of the point-charge model of the c.f. potential, that the major displacements are those of the Sm^{2+} ion and the cation vacancy toward each other.

Consideration must be given to the various sources of error in the calculated c.f. coefficients which arise from the use of point-charge models. It was pointed out earlier that the major contribution to the potential field at the Sm^{2+} ion arises from the n.n. halide ions and the cation vacancy. The rest of the lattice contributes only a small fraction of the total crystal field. It appears, therefore, unlikely that displacements of next-nearest neighbors will change the qualitative picture developed from the n.n. displacements alone. The observation that the c.f. splitting is essentially the same in RbCl and KCl gives support to this hypothesis. Similarly, the observation that the energies of the $4f^6$ states of Sm^{2+} are essentially the same in a number of the alkali halides, alkaline-earth halides, as well as in other crystals, seems to indicate that the influence of covalency effects is small for this configuration.

It is by no means as certain that induced dipole and multipole effects can be neglected. In general, the induced dipole on the halide ions ought to be smaller than that estimated by Hutchings and Ray[25] for Pr^{3+} in $LaCl_3$, because the effective charge of the Sm^{2+} is smaller than that of Pr^{3+} or La^{3+}. In this connection it is interesting to note that the splittings are smaller in KBr than in KCl, and that the ratio of the c.f. coefficients is not significantly different from those expected from a point-charge model modified to take account of the increased shielding of the vacancy and lattice potential by the greater polarizability of KBr.

A number of authors[26–29] have shown that another possible source of error in a point-charge model involves distortions of the wave functions of the $4s$, $4p$, and particularly of the $5s$ and $5p$ shielding electrons, by the external crystal field. For Pr^{3+}, the various authors appear to agree that this effect amounts to a 25–50% reduction of A_2^0 and that it is smaller for higher harmonics. Such a reduction should also apply to A_2^2. Hence this effect should not disturb the present qualitative conclusions on ion displacements, which are based on ratios of coefficients of the same order in ν.

Watson and Freeman[30] have recently pointed out that for open-shell rare-earth ions, such as Sm^{2+}, there will arise an additional shielding effect. This consists of a difference in the distortion (from one m_l value to another) due to the virtual excitation of closed-shell electrons of orbital angular momentum l to f orbitals of varying m_l. Such a difference would be particularly important for very strong low-symmetry fields. It would in general cause the splittings of levels of given J to

[25] M. T. Hutchings and D. K. Ray, Proc. Phys. Soc. (London) 81, 663 (1963).

[26] C. J. Lenander and E. Y. Wong, J. Chem. Phys. 38, 2750 (1963).

[27] G. Burns, Phys. Rev. 128, 2121 (1962).

[28] D. K. Ray, Proc. Phys. Soc. (London) 82, 47 (1962).

[29] A. J. Freeman and R. E. Watson, Phys. Rev. 127, 2058 (1962).

[30] R. E. Watson and A. J. Freeman, Phys. Rev. 133, A1571 (1964).

vary considerably from those determined by an external potential alone.

There is no very good evidence that such subtle influences are at work in the present study. The $5s$ and $5p$ orbitals used to show the quantitative importance of these effects extend in any case over neighboring ions, so that if the effects are important, they should cause a difference in the ratios of the various crystal-field parameters obtained for the case of chloride as against bromide n.n. ions. The same reasoning should apply upon a change of next-nearest neighbors from potassium to rubidium ions. In contrast, nothing extremely inconsistent with simple displacement and polarization effects can be detected in the present data, although a subsequent examination of the data for higher J might show up further relevant evidence on these points. Perhaps another useful experiment, to check the magnitude of these effects, would be the comparison of the c.f. splittings of another divalent ion of a different f^n configuration, such as Tm^{2+}, to that of Sm^{2+}.

It should be mentioned that the influence of $J-J'$ mixing has been estimated, using Ofelt's[31] intermediate-coupling wave functions for the f^6 configuration. It was found to contribute only a small amount (of the order of several reciprocal centimeters) to the splittings, although it may contribute to the intensities of the various components. For example, the weak magnetic-dipole transition $^5D_0(A_1) \rightarrow {}^7F_2(A_2)$ would only be observed if $J-J'$ admixture occurs among the states of the $4f^6$ configuration.

Finally, attention should be called to the intensities of the other components in the transitions $^5D_0 \rightarrow {}^7F_{0,1,2}$. In the work of Wood and Kaiser (SrF_2),[14] and that of Axe and Sorokin ($SrCl_2$),[32] very little intensity was found in the $^5D_0(A_{1g}) \rightarrow {}^7F_0(A_{1g})$ transition of Sm^{2+}. The cubal symmetry of these lattices forbids, however, electric dipole (as well as magnetic dipole) transitions between two states of A_{1g} symmetry. In C_{2v} symmetry, on the other hand, an electric dipole transition can occur between states of A_1 symmetry (see Table IV). Observation of this transition as an electric dipole transition, as well as electric-dipole transitions to various components of the other ^7F_J states, is a direct consequence of the lack of inversion symmetry. The relatively high intensity of the $^5D_0 \rightarrow {}^7F_0$ transition [compared for example to Eu^{3+} in CdF_2 (Ref. 16) or $LaCl_3$ (Ref. 17)] indicates, in addition, a strong admixture to the $^5D_0$ state of higher excited states with $J=1$ and of A_1 symmetry. Presumably this occurs through the V_1^0 part of the crystal field. It is somewhat more difficult to understand why the transitions $^5D_0(A_1) \rightarrow {}^7F_1(B_1)$ and $^5D_0(A_1) \rightarrow {}^7F_1(B_2)$ are magnetic-dipole transitions and not electric-dipole transitions. Both types of transitions are allowed by symmetry considerations alone. Magnetic-dipole transitions would be predicted to dominate if the calculations of the intensities by Ofelt[33] and of Judd[34] could be applied to the present case. The closure procedure used in these calculations, to obtain the influence of configurations of opposite parity requires, however, that a large energetic difference exist between these configurations and the $4f^n$ configuration. Although this is not the case for Sm^{2+}, it is rather suggestive that the results of the closure procedure appear to be valid for the $J=0$ to $J=1$ transitions.

A quantitative theoretical treatment of the displacements of the lattice ions surrounding the Sm^{2+} and its associated vacancy should now be possible along the lines originally used by Bassani and Fumi, and modified in principle by Hardy.[35] Recent work on the lattice absorption spectra of the alkali halides[36] encourages one to believe that the force constants and polarizabilities involved can be estimated with sufficient accuracy to make a more sophisticated treatment of the defect worthwhile.

ACKNOWLEDGMENT

The authors wish to thank Dr. J. D. Axe, Dr. R. W. Dreyfus, and Dr. A. S. Nowick for many helpful discussions. The computer program was developed by Dr. R. P. Kelisky and programmed by Mrs. J. Somorjai.

[31] G. S. Ofelt, J. Chem. Phys. **38**, 2171 (1963).
[32] J. D. Axe and P. P. Sorokin, Phys. Rev. **130**, 945 (1963).
[33] G. S. Ofelt, J. Chem. Phys. **37**, 511 (1962).
[34] B. R. Judd, Phys. Rev. **127**, 750 (1962).
[35] J. R. Hardy, Phys. Chem. Solids **15**, 39 (1960); **23**, 113 (1962).
[36] A. D. B. Woods, W. Cochran, and B. N. Brockhouse, Phys. Rev. **119**, 980 (1960).